Diffusion parameters in single-crystalline Li_3N as probed by ^6Li and ^7Li spin-alignment echo NMR spectroscopy in comparison with results from ^8Li β-radiation detected NMR

2008 J. Phys.: Condens. Matter 20 022201

(http://iopscience.iop.org/0953-8984/20/2/022201)

IOP FTC
IOP PUBLISHING JOURNAL OF PHYSICS: CONDENSED MATTER
J. Phys.: Condens. Matter **20** (2008) 022201 (5pp) doi:10.1088/0953-8984/20/02/022201

FAST TRACK COMMUNICATION

Diffusion parameters in single-crystalline Li_3N as probed by ^6Li and ^7Li spin-alignment echo NMR spectroscopy in comparison with results from ^8Li β-radiation detected NMR

Martin Wilkening, Denis Gebauer[1] and Paul Heitjans

Institute of Physical Chemistry and Electrochemistry, Leibniz University Hannover, Callinstrasse 3-3a, 30167 Hannover, Germany

E-mail: wilkening@pci.uni-hannover.de and heitjans@pci.uni-hannover.de

Received 17 October 2007, in final form 6 November 2007
Published 6 December 2007
Online at stacks.iop.org/JPhysCM/20/022201

Abstract

^6Li and ^7Li two-time spin-alignment echo NMR correlation functions of single-crystalline Li_3N are recorded. Around room temperature, the decay of the spin-alignment echo amplitudes is induced by slow Li jumps perpendicular to the Li_2N layers. The hopping correlation functions can be best represented by a single exponential. The measured jump rates are consistent with those which were previously determined by ^8Li β-radiation detected NMR at much lower temperatures. Taking the results from ^6Li and ^7Li NMR as well as from ^8Li β-NMR together, between 360 and 220 K Arrhenius behaviour is found. The corresponding activation energy is 0.65(1) eV and the pre-exponential factor turned out to be $6.4(5) \times 10^{13}$ s^{-1}. Although probed from a microscopic point of view, the NMR diffusion parameters are in very good agreement with those obtained from dc-conductivity measurements, being sensitive to macroscopic transport properties.

1. Introduction

Currently, there is an increasing interest in developing new solid state Li ion batteries with high energy density [1, 2]. In particular, fast Li conductors are required which serve as potential solid electrolytes [3]. This interest is accompanied by the perpetual effort to develop new experimental methods which are useful to measure microscopic Li diffusion parameters such as jump rates and activation energies. Unfortunately, due to the lack of a suitable radioactive Li isotope the tracer method [4], which is the standard technique to measure macroscopic diffusion coefficients, cannot be applied. Alternatively, nuclear magnetic resonance (NMR) techniques [5–9] are highly suitable to compensate for this methodological lack. In the present paper, Li diffusion in single-crystalline Li_3N, which serves as a model substance, is investigated by both ^6Li and ^7Li two-time spin-alignment echo (SAE) NMR spectroscopy. SAE-NMR allows the direct measurement of microscopic Li jump rates with values in the kHz range. Li diffusion parameters in single-crystalline Li_3N are well known especially from the various measurements using traditional NMR techniques; see, e.g., [10–14]. The results obtained here are compared with previously measured Li jump rates at temperatures smaller than 260 K [15] using the ^8Li β-radiation detected NMR method [7].

Whereas in a number of papers ^7Li SAE-NMR was used in recent years [8, 16–26] to investigate Li dynamics by two-

[1] Present address: Max-Planck-Institute of Colloids and Interfaces, Am Mühlenberg 1, D-14424 Potsdam, Germany.

time correlation functions, to our knowledge the generation of ^{6}Li NMR spin-alignment echoes has not been reported so far. ^{6}Li sin–sin NMR correlation functions were probed first in [27], on which this paper is based. A brief comparison of ^{7}Li spin-alignment correlation functions with ^{6}Li cos–cos hopping correlation functions was first presented in [8]. If applicable, the ^{6}Li SAE-NMR technique shows several advantages over ^{7}Li SAE-NMR. Whereas the spin-quantum number I of ^{7}Li is 3/2, the ^{6}Li isotope is— like ^{2}H—a spin-1 nucleus. It is known that ^{2}H SAE-NMR [28] is one of the most powerful NMR methods to probe translational as well as rotational jump rates in condensed matter [28–31]. It takes advantage of the quadrupole interaction between the quadrupole moment Q of the nucleus and a non-vanishing electric field gradient (EFG) produced by the charge distribution in the neighbourhood of the ion. ^{7}Li and ^{2}H have comparable Q values leading in many solids to quadrupole coupling constants δ with values in the kHz range, which is a necessary pre-condition to apply SAE-NMR because a non-selective excitation of the entire SAE-NMR spectrum is required. The quadrupole moment of ^{6}Li (−0.818(17) mb) [32] is by a factor of 50 smaller than that of ^{7}Li (−40.6(9) mb) [32]. However, in Li_3N the exceptionally large field gradients at the Li sites (see below) lead to values of δ in the kHz range even for the ^{6}Li nucleus. This offers the possibility to perform ^{6}Li spin-alignment NMR experiments analogous to those for ^{2}H. The much smaller magnetic moment of ^{6}Li as compared to that of the ^{7}Li nucleus is beneficial for spin-alignment NMR because interfering homonuclear dipolar interactions [18] are nearly absent. Moreover, as ^{6}Li is a spin-1 nucleus the record of multi-time correlation functions might be possible, which are extremely difficult to measure in the case of ^{7}Li [33]. Although the natural abundance of ^{6}Li is only 7.42% (^{7}Li: 92.58%), in the case of Li_3N a strong ^{6}Li NMR signal was obtained without further isotope enrichment. Thus, Li_3N serves as a first test substance to use ^{6}Li two-time SAE-NMR spectroscopy for the direct observation of slow Li jump processes in a solid ionic conductor.

The layered crystal structure of Li_3N (space group $P6/mmm$) is depicted in figure 1. The nitrogen N^{3-} anions occupy the corners of the elementary cell. They are each bipyramidally surrounded by eight Li atoms. The six Li ions within the ab-plane are usually labelled as Li(2). They are involved in the fast intralayer diffusion process responsible for the very high room temperature Li conductivity of Li_3N (10^{-4} S cm^{-1}), cf e.g. [34–37]. The Li ions between the Li_2N layers, Li(1), are much less mobile. The transport process parallel to the c-axis, which is called the interlayer diffusion process, shows a Li conductivity which is about two to three orders of magnitude smaller than that perpendicular to it; see, e.g. [13, 14, 34–37]. Li ions involved in this diffusion process are exposed to two distinct crystallographic positions with different quadrupole coupling constants. At ambient temperature a Li jump rate of the order of 10^3 s^{-1} is expected. This value lies in the typical dynamic range to which spin-alignment echo NMR is sensitive. Thus, it should be possible to detect the room temperature Li exchange (Li(1) ↔ Li(2)) between the two electrically inequivalent Li sites in Li_3N by SAE-NMR.

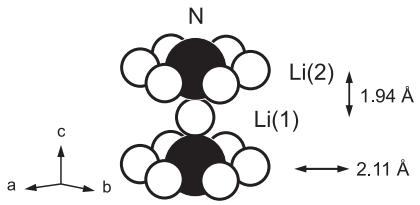

Figure 1. Crystal structure of Li_3N. Two electrically inequivalent Li sites are present: The Li(2) ions are involved in a fast intralayer diffusion process, whereas the Li ions on Li(1) positions are exchanged perpendicular to the ab-plane.

2. Experimental details

^{6}Li and ^{7}Li spin-alignment echoes were recorded via the three-pulse sequence introduced by Jeener and Broekaert [38] ($90^\circ_{\phi_1}$–t_p–$45^\circ_{\phi_2}$–t_m–$45^\circ_{\phi_3}$–t–echo) leading to sin–sin correlation functions. Furthermore, we have used the stimulated echo pulse sequence ($90^\circ_{\phi_5}$–t_p–$90^\circ_{\phi_6}$–t_m–$90^\circ_{\phi_7}$–t–echo) to monitor cos–cos two-time correlation functions. The evolution time t_p was fixed (15 μs). The mixing time t_m was varied between 5 μs and 1 s. Appropriate cycling of the phases ϕ_i ensures the desired coherence [18, 29, 33]. The recycle delay between the scans was $6T_1$, where T_1 is the corresponding spin–lattice relaxation time. An MSL 400 NMR spectrometer (Bruker) in connection with an Oxford cryomagnet (89 mm, wide bore) at fixed field B_0 of about 9.4 T was used. This magnetic field corresponds to the resonance frequencies $\omega_0/2\pi(^7\text{Li}) = 155$ MHz and $\omega_0/2\pi(^6\text{Li}) = 58$ MHz, respectively. The 90° pulse lengths were 4.5 μs for the ^{7}Li and 8.5 μs for the ^{6}Li experiments. The temperature in the probe was controlled by an Oxford ITC in combination with a Ni–CrNi thermocouple. We have employed a standard solid-state NMR probe from Bruker. Solid echo spectra were acquired using the solid echo pulse sequence (90°–t_e–R–t–echo). In order to maximize the echo signal, R was chosen to be either a 90° (^{6}Li) or a 64° (^{7}Li) pulse. The interpulse delay t_e was set to about 20 μs.

3. Results and discussion

In figure 2 ^{6}Li solid echo NMR spectra of single-crystalline Li_3N are shown for various temperatures. As can be clearly seen, the interlayer diffusion process causes a nearly complete coalescence of the ^{6}Li resonance lines with increasing temperature. As expected, at low T two pairs of resonances with different quadrupole splittings can be well resolved. Note that also the centres of gravity of the two resonance pairs of figure 2 do not coincide due to different environments of the Li ions. The two pairs represent the Li ions within (Li(2)) and between the Li_2N layers (Li(1)), respectively. Intralayer Li ions are exposed to an electric field gradient (EFG) which is by about a factor of two smaller than that for Li within the layers, see e.g. [10, 15, 39]. In both cases the EFG is axially symmetric [39]. From the different splittings the following ^{6}Li quadrupole coupling constants δ are obtained: $|\delta_{\text{Li}(1)}| = 12.04$ kHz and $|\delta_{\text{Li}(2)}| = 5.67$ kHz. This is in good agreement with results reported earlier (11.7 and 5.7 kHz, see [10, 40]). Whereas the Li(2) resonance lines are already

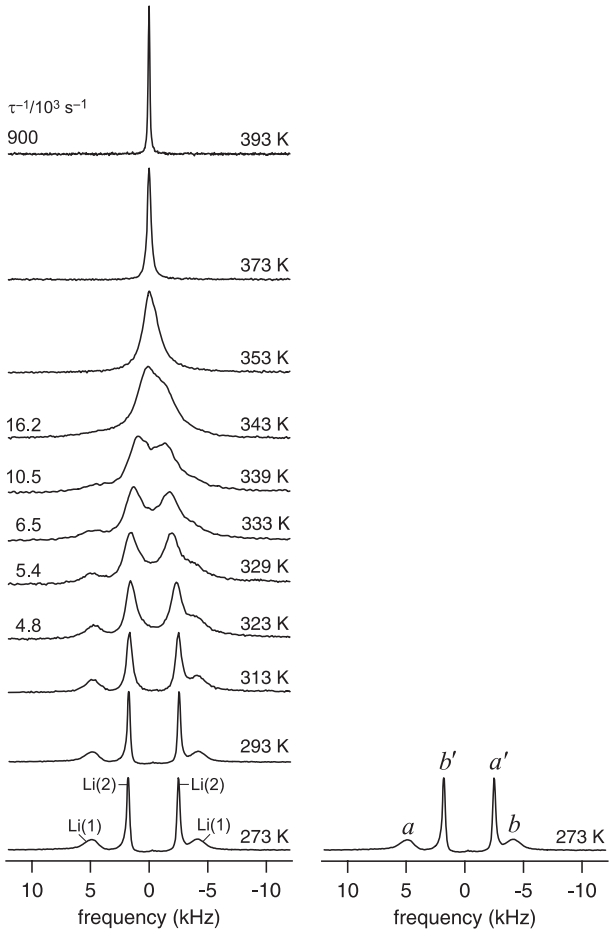

Figure 2. ^{6}Li solid echo spectra of single-crystalline Li_3N recorded at the temperatures indicated, $c \perp B_0$. Coalescence of the resonances is observed at elevated temperatures. NMR lines corresponding to each other are marked with a, a' and b, b', respectively (see text).

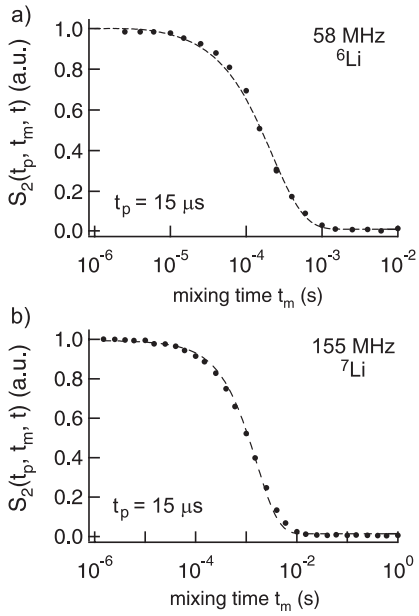

Figure 3. (a) ^{6}Li spin-alignment echo amplitudes S_2 as a function of mixing time t_m and for a constant evolution time $t_p = 15$ μs. The dashed line shows a fit with a single-exponential function. The amplitudes were recorded at a resonance frequency of 58 MHz and at $T = 328$ K. (b) ^{7}Li spin-alignment echo amplitudes S_2 measured at 293 K and under the same conditions as for ^{6}Li. Again, the echo decay follows a single exponential. See figure 4 for a comparison of the resultant jump rates from the ^{6,7}Li SAE-NMR experiments.

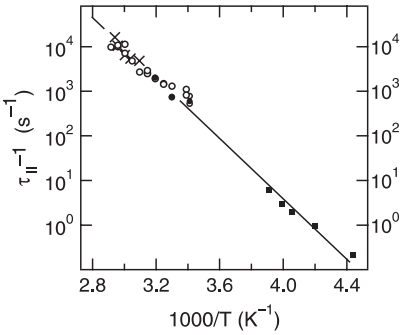

Figure 4. Li jump rates ($\tau^{-1} = \tau_{\parallel}^{-1}$) obtained from ^{6}Li solid echo NMR spectra (×), ^{6}Li (○) and ^{7}Li SAE-NMR (●) as well as from ^{8}Li spin–lattice relaxation β-NMR transients (■). The latter were taken from [15]. $\tau_{\parallel}^{-1}$ characterizes interlayer hopping of Li^+ in Li_3N, i.e. parallel to the c-axis. The Arrhenius fit (solid line) yields $E_a = 0.65(1)$ eV and $\tau_0^{-1} = 6.4(5) \times 10^{13}$ s^{-1}.

motionally narrowed at $T = 273$ K due to the fast intralayer diffusion process, the outer NMR lines are still broadened because of the much smaller diffusivity of the interlayer Li(1) ions. Coalescence of the resonances is observed when the interlayer jump rate τ^{-1} reaches a value of the order of the distance (several kilohertz) between the NMR resonance lines. The fact that no ^{6}Li doublet is found at the highest T indicates that the EFGs of the two different Li sites have different signs. This was determined experimentally by β-NMR [15, 41] previously and is in agreement with theoretical investigations [39]. The resonance lines corresponding to each other are marked in figure 2 with a, a' and b, b', respectively. Taking into account the number of Li(1) and Li(2) ions in Li_3N, this yields by means of $\bar{\delta}_{\mathrm{Li}(1),\mathrm{Li}(2)} = \frac{1}{3}\delta_{\mathrm{Li}(1)} + \frac{2}{3}\delta_{\mathrm{Li}(2)}$ and $\delta_{\mathrm{Li}(1)}/\delta_{\mathrm{Li}(2)} \approx -2.1$ a residual quadrupole splitting $|\bar{\delta}_{\mathrm{Li}(1),\mathrm{Li}(2)}|$ of about 0.2 kHz. In fact, we were able to resolve a quadrupole splitting of 51 Hz at 418 K [27]. This value is smaller than expected and points to the fact that the EFGs decrease slightly with increasing temperature [15].

We have used a rather simple formalism for a rough determination of Li jump rates (see figure 4) from the ^{6}Li solid echo spectra shown in figure 2. Below about 340 K the jump rate τ^{-1} is obtained via the expression $\tau^{-1} \approx \pi\Delta\nu$ [42], where $\Delta\nu$ is the lifetime broadening of the resonance line. At higher T, when coalescence is starting, the rate is approximately given by $\tau^{-1} \approx (\pi/\sqrt{2})\Delta\nu_{b',b}$ [42], where $\Delta\nu_{b',b} = \nu_{b'} - \nu_b$. In the regime of fast Li exchange (400 K) we have estimated the jump rate according to $\tau^{-1} \approx 4\pi\frac{1}{3}\frac{2}{3}(\Delta\nu_{b',b})^2/\Delta\nu$, where the population of the Li(1) and Li(2) sites is taken into account [42]. The so-obtained rates are in reasonable agreement with those which were directly obtained from ^{6}Li two-time correlation functions (see below and figure 4). In figure 3(a) ^{6}Li spin-alignment echo amplitudes recorded at $t_p = 15$ μs and 328 K are shown versus mixing time

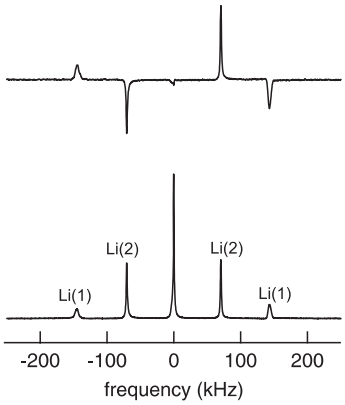

Figure 5. Top: pure ^{7}Li quadrupolar spin-alignment echo NMR spectrum recorded at 293 K and a resonance frequency of 155 MHz. $t_p = 13.8$ μs and $t_m = 10.0$ μs. Bottom: ^{7}Li solid echo spectrum at 293 K and 155 MHz. The interpulse delay t_e was set to 10.0 μs. Both spectra were recorded for $c \perp B_0$.

t_m. The corresponding ^{7}Li spin-alignment echo decay curve (see below) is displayed in figure 3(b) for comparison. The amplitudes are scaled such that they range between 0 and 1. The echo decay is induced by slow Li jumps between the electrically inequivalent Li sites (1) and (2). Due to the different quadrupole coupling constants $\delta_{\mathrm{Li}(i)}$ ($i = 1, 2$) which the ions possess, they are individually labelled by the (angular) quadrupole frequencies $\omega_Q(\mathrm{Li}(1))$ and $\omega_Q(\mathrm{Li}(2))$, respectively. ω_Q becomes a function of t_m due to slow interlayer Li hopping. By means of two-time spin-alignment echo NMR the quadrupole frequency at $t = t_m = 0$ is correlated with that at a later time $t = t_m$. Applying the pulse lengths mentioned in section 2, in the present case we have recorded ^{6}Li and ^{7}Li sin–sin as well as ^{6}Li cos–cos hopping correlation functions. Within the experimental error the ^{6}Li NMR experiments gave the same jump rates at the evolution times employed here. The sin–sin correlation function is given by $S_2 \propto \sin(\omega_Q(t = 0)t_p)\sin(\omega_Q(t = t_m)t_p)$. The dashed lines in figure 3 represent fits with exponential functions, $S_2(t_p, t_m, t = t_p) \propto \exp -(\tau/t_m)$. At $T = 328$ K the decay rate τ^{-1} is $4.6(2) \times 10^3$ s^{-1}.

In general, the echo amplitude S_2 is additionally damped by other processes. Quadrupolar order decays simply due to quadrupolar spin–lattice relaxation [8, 25] or spin-diffusion effects [8]. However, the latter is temperature independent and proceeds on a timescale with rates of the order of 1 s^{-1}. In the temperature range which was covered for the spin-alignment NMR measurements the spin–lattice relaxation rates are of the order of about 0.1 s^{-1}. Therefore, the S_2 decay shown in figure 3 is exclusively induced by slow Li jumps. The above mentioned jump rate corresponds to an Li residence time of about $2.16(9) \times 10^{-4}$ s at 328 K. Increasing temperature shifts the decay curves to smaller mixing times. The shape of the correlation functions remains unchanged. Above 350 K the Li ions are exposed to the quadrupole coupling constant $\bar{\delta}$ (see above). In this temperature range the associated very small changes of ω_Q (which differ on the Hz scale, see above) can no longer be resolved by using a short t_p of only 15 μs. Therefore, ω_Q becomes quasi-independent of t_m. This temperature determines the upper limit of a reliable detection of jump rates by ^{6}Li SAE-NMR. It was verified that the measured decay rate is independent of the crystal orientation. This is expected for a Li jump rate which should also be independent of the resonance frequency $\omega_0/2\pi$ used. The ^{6}Li spin-alignment jump rates are shown together with the rates estimated from the ^{6}Li solid echo NMR spectra in figure 4. In order to further verify that the ^{6}Li spin-alignment NMR decay rates are equal to Li jump rates, analogous experiments using the ^{7}Li isotope can be done, which should result in the same values, provided pure spin-alignment order can also be generated for the spin-3/2 nucleus. Only in this case a single-particle correlation function like that in the ^{6}Li case is obtainable. By applying ^{7}Li spin-alignment echo NMR the simultaneous creation of dipolar order should not be underestimated [17, 22]. Note that it is almost negligible for ^{6}Li NMR experiments. In the worst case this would lead to ^{7}Li multi-particle correlation functions, which result in larger jump rates than expected. However, it was shown that by the use of small evolution times ^{7}Li–^{7}Li dipolar contributions to the spin-alignment echo are greatly reduced [17, 22]. In the present case we have the very beneficial situation that the quadrupole couplings in Li_3N are much larger than the dipolar ones. In figure 5 the ^{7}Li spin-alignment echo and the corresponding solid echo NMR spectrum of single-crystalline Li_3N are shown. The spectra were recorded at 293 K and a ^{7}Li resonance frequency of $\omega_0/2\pi = 155$ MHz. Inspection of the central line of the solid echo spectrum in more detail reveals that it is composed of two NMR lines: a motionally narrowed sharp and a less intense broad line reflecting the Li(2) and Li(1) ions, respectively, see [27]. The different widths of the satellite lines also represent the two different diffusion processes in Li_3N. The respective quadrupole splittings lead to ^{7}Li quadrupole couplings constants of 284(1) kHz and 581(2) kHz for the two Li sites. These values are in good agreement with those reported earlier [10, 13]. Using the above mentioned results from ^{6}Li NMR the ratio of the quadrupole moments $Q(^6\mathrm{Li})/Q(^7\mathrm{Li})$ is about 0.02. With respect to the error of $\pm 10°$ concerning the mis-orientation of the crystal in the magnetic field, this result is in good agreement with literature values. Altogether, the error of the ratio $Q(^6\mathrm{Li})/Q(^7\mathrm{Li})$ is about ± 0.004.

The ^{7}Li spin-alignment echo NMR spectrum in figure 5 was recorded at $t_p = 13.8$ μs in order to observe all satellite lines, which are each modulated by $\sin(\omega_Q(\mathrm{Li}(i))t_p)$. The central lines are completely absent, indicating the generation of pure quadrupolar order after the first two radio frequency pulses. A short mixing time ensures that the spectrum is not affected by Li diffusion. It clearly exhibits the opposite signs of the two coupling constants in Li_3N [15, 39, 41]. Corresponding NMR lines of the spin-alignment spectrum in figure 5 have either positive or negative intensities.

The decay of the ^{7}Li NMR S_2 amplitude with increasing mixing time is shown in figure 3(a). Similar to the ^{6}Li decay curves it follows a pure exponential. The decay rate at $T = 293$ K is $6.2(2) \times 10^2$ s^{-1}. This value is in good agreement with the rates directly obtained by ^{6}Li spin-alignment echo NMR (see figure 4). In the Arrhenius plot of figure 4, Li jump

rates of the interlayer diffusion process in Li_3N from ^8Li β-radiation detected NMR are also included. These rates were obtained via an analysis of the diffusion induced ^8Li spin–lattice relaxation transients by measurements of our group in former times on a similar sample. We refer to [15] for experimental details. Finally, we can identify the jump rates (τ^{-1}) measured here with those characterizing the interlayer hopping process in Li_3N ($\tau_{\parallel}^{-1}$). The rates are consistent with the present results, as is shown by the solid line in figure 4. It represents a fit according to $\tau^{-1} = \tau_0^{-1} \exp(-E_a/k_B T)$, where k_B is the Boltzmann constant, which yields an activation energy E_a of 0.65(1) eV and a pre-exponential factor τ_0^{-1} of $6.4(5) \times 10^{13}$ s^{-1}. E_a is in very good agreement with results which were obtained by the investigation of the temperature dependence of the dc conductivity (σ_{dc}) and by various NMR techniques. These values mainly range between 0.59 and 0.67 eV; see, e.g. [36] and [10]. As an example, in [36] an activation energy of 0.67(3) eV and a pre-factor of $\approx 1 \times 10^{14}$ s^{-1} were obtained ($\sigma_{dc} \parallel c$). Thus, besides the very recent NMR investigations of Li diffusion in polycrystalline Li_7BiO_6 [26] and $Li_4Ti_5O_{12}$ [24] the present paper is another example where ^6Li as well as ^7Li SAE-NMR turned out to be a reliable and easily applicable tool for the microscopic determination of long-range diffusion parameters.

4. Conclusion

In this study, two-time $^{6,7}Li$ spin-alignment echo NMR was employed to probe microscopic diffusion parameters of the interlayer Li^+ hopping in single-crystalline Li_3N, which served as a model substance. The Li jump rates agree well with results from ^8Li β-radiation detected NMR which were obtained at much lower temperatures. Altogether, Arrhenius behaviour over a dynamic range of five orders of magnitude is found. The results agree well with literature values from dc-conductivity measurements probing macroscopic Li transport. The present investigation emphasizes that spin-alignment echo NMR—applied to both the ^6Li and ^7Li nuclei—is on its way to become an interesting and reliable alternative for conventional macroscopic techniques in general as well as for well established NMR methods in particular.

Acknowledgments

We thank C T Lin (Max-Planck Institute for Solid State Research, Stuttgart, Germany) for the Li_3N single crystals. Financial support by the Deutsche Forschungsgemeinschaft (DFG) is gratefully acknowledged.

References

[1] Tarascon J M and Armand M 2001 *Nature* **1414** 359
[2] Whittingham M S 2004 *Chem. Rev.* **104** 4271
[3] Adachi G, Imanaka N and Aono H 1996 *Adv. Mater.* **8** 127
[4] Mehrer H 2005 *Diffusion in Condensed Matter—Methods, Materials, Models* 2nd edn, ed P Heitjans and J Kärger (Berlin: Springer) chapter 1, pp 3–64
[5] Brinkmann D 1992 *Prog. Nucl. Magn. Reson. Spectrosc.* **24** 527
[6] Heitjans P, Indris S and Wilkening M 2005 *Diffus. Fundam.* **2** 45 (online journal: www.diffusion-fundamentals.org)
[7] Heitjans P, Schirmer A and Indris S 2005 *Diffusion in Condensed Matter—Methods, Materials, Models* 2nd edn, ed P Heitjans and J Kärger (Berlin: Springer) chapter 9, pp 369–415
[8] Böhmer R, Jeffrey K and Vogel M 2007 *Prog. Nucl. Magn. Reson. Spectrosc.* **50** 87
[9] Heitjans P and Indris S 2003 *J. Phys.: Condens. Matter* **15** R1257
[10] Brinkmann D, Mali M, Roos J, Messer R and Birli H 1982 *Phys. Rev.* B **26** 4810
[11] Brinkmann D, Mali M, Roos J and Messer R 1981 *Solid State Ion.* **5** 409
[12] Bechthold-Schweickert E, Mali M, Roos J and Brinkmann D 1984 *Phys. Rev.* B **30** 2891
[13] Brinkmann D, Freudenreich W and Roos J 1978 *Solid State Commun.* **28** 233
[14] Messer R, Birli H and Differt K 1981 *J. Phys. C: Solid State Phys.* **14** 2731
[15] Bader B, Heitjans P, Stöckmann H-J, Ackermann H, Buttler W, Freiländer P, Kiese G, van der Marel C and Schirmer A 1992 *J. Phys.: Condens. Matter* **4** 4779
[16] Böhmer R, Jörg T, Qi F and Titze A 2000 *Chem. Phys. Lett.* **316** 419
[17] Qi F, Jörg T and Böhmer R 2002 *Solid State Nucl. Magn. Reson.* **22** 484
[18] Qi F, Diezemann G, Böhm H, Lambert J and Böhmer R 2004 *J. Magn. Reson.* **169** 225
[19] Qi F, Rier C, Böhmer R, Franke W and Heitjans P 2005 *Phys. Rev.* B **72** 104301
[20] Wilkening M and Heitjans P 2005 *Defect Diffus. Forum* **237–240** 1182
[21] Wilkening M, Küchler W and Heitjans P 2006 *Phys. Rev. Lett.* **97** 065901
[22] Wilkening M and Heitjans P 2006 *J. Phys.: Condens. Matter* **18** 9849
[23] Wilkening M and Heitjans P 2006 *Solid State Ion.* **177** 3031
[24] Wilkening M, Amade R, Iwaniak W and Heitjans P 2007 *Phys. Chem. Chem. Phys.* **9** 1239
[25] Böhmer R and Qi F 2007 *Solid State Nucl. Magn. Reson.* **31** 28
[26] Wilkening M, Mühle C, Jansen M and Heitjans P 2007 *J. Phys. Chem.* B **111** 8691
[27] Wilkening M 2005 *PhD Thesis* University of Hannover
[28] Spiess H W 1980 *J. Chem. Phys.* **72** 6755
[29] Lausch M and Spiess H W 1983 *J. Magn. Reson.* **54** 466
[30] Fujara F, Wefing S and Spiess H W 1986 *J. Chem. Phys.* **84** 4579
[31] Dries T, Fujara F, Kiebel M, Rössler E and Silescu H 1988 *J. Chem. Phys.* **88** 2139
[32] Cederberg J, Olson D, Larson J, Rakness G, Jarausch K, Schmidt J, Borovsky B, Larson P and Nelson B 1998 *Phys. Rev.* A **57** 2539
[33] Böhmer R 2000 *J. Magn. Reson.* **147** 78
[34] Bourkamp B A and Huggins R A 1976 *Phys. Lett.* A **58** 231
[35] Alpen U v, Rabenau A and Talat G H 1977 *Appl. Phys. Lett.* **30** 621
[36] Wahl J 1979 *Solid State Commun.* **29** 485
[37] Wahl J and Holland U 1978 *Solid State Commun.* **27** 237
[38] Jeener J and Broekaert P 1967 *Phys. Rev.* **157** 232
[39] Blaha P, Schwarz K and Herzig P 1985 *Phys. Rev. Lett.* **54** 1192
[40] Brinkmann D, Mali M and Roos J 1979 *Proc. Int. Conf. on Fast Ion Transport in Solids* (New York: North-Holland) p 483
[41] Bader B, Heitjans P, Ackermann H, Freiländer P, Kiese G, Schirmer A, Stöckmann H-J and van der Marel C 1985 *Ann. Phys., Lpz.* **42** 169
[42] Hore P J 2002 *Nuclear Magnetic Resonance* (New York: Oxford University Press)